Nonlinear State Estimation and Model Predictive Control of Nitrogen Purification Columns

Shoujun Bian and Michael A. Henson*

Department of Chemical Engineering, University of Massachusetts, Amherst, Massachusetts 01003-9303

Paul Belanger and Lawrence Megan

Process and Systems Research and Development, Praxair, Inc., Tonawanda, New York 14051-7891

Nitrogen purification columns are critical unit operations of air separation plants that produce purified gases for the chemical, steel, food processing, medical, and semiconductor industries. The need to operate these very high purity columns over a wide range of production rates in response to time-varying electrical costs motivates the development of nonlinear control strategies. We utilize a nonlinear wave model previously developed by our group to design a nonlinear model predictive controller for a simulated nitrogen purification column. A first principles model constructed in Aspen Dynamics (Aspen Technology) is used as a surrogate plant in the simulation studies. Estimates of the unmeasured wave position and key wave model parameters are generated with an extended Kalman filter using a combination of composition and temperature measurements strategically placed along the column. Several estimator formulations are investigated to evaluate the effects of different measurement combinations. The estimator and predictive controller are combined through a state disturbance model that provides feedback and eliminates offset due to modeling errors. The controller manipulates the vapor nitrogen production rate to achieve the target nitrogen purity. The proposed control strategy is compared to a classical control system consisting of a ratio controller and a proportional−integral−derivative controller to analyze the potential benefits of nonlinear model-based control for this process.

1. Introduction

Cryogenic distillation is used to produce large quantities of purified nitrogen, oxygen, argon, and rare gases for the steel, chemical, food processing, semiconductor, and health care industries.[3,13] Cryogenic distillation columns are operated at extremely low temperatures (−170 to −190 °C) to separate air components according to their different boiling temperatures. Purified streams are produced in liquid and/or gaseous states for transportation to end users. The major operating cost associated with cryogenic air separation plants is electricity. The domestic consumption of electricity by industrial gas producers is over $700 million/year. Therefore, small improvements in process control have the potential to result in substantial economic benefits.

Current state-of-the-art control technology in the air separation industry is based on linear dynamic models and linear model predictive control.[24,40] Despite the very high product purities required, linear control technology has proven to be successful because cryogenic distillation columns typically operate over a small range of production rates. Deregulation of the electric utility industry is expected to lead to frequent and unpredictable changes in the cost of electricity, which mandate fundamental changes in the operating philosophy of air separation plants. An obvious strategy is to maximize production when electricity is relatively inexpensive and to minimize production when electricity costs are high. Column nonlinearities will become much more pronounced under these operating conditions, and some type of nonlinear control may be necessary to achieve a satisfactory performance.

The availability of a suitable nonlinear dynamic model is a prerequisite for the development of a nonlinear control strategy. Fundamental distillation column models are comprised of stage-by-stage mass and energy balances combined with hydraulic relations for the liquid holdup on each stage.[20] A distillation column with N equilibrium stages and n components is described by $N(n + 1)$ nonlinear differential equations plus nonlinear algebraic equations for the hydraulic and vapor−liquid equilibrium relations. Even under simplifying assumptions such as a binary (or pseudobinary) mixture, equal molar overflow, and constant molar holdup, N differential equations are required to model the column dynamics. For nitrogen purification columns with approximately 50 equilibrium stages, the high model dimension is a major obstacle to nonlinear controller design and implementation.

We previously developed a low-order dynamic modeling technique for nitrogen purification columns based on nonlinear wave theory.[44] The basic premise of nonlinear wave modeling is that the concentration or temperature profile of a distillation column can be described by a moving wave front with a constant pattern.[12,16,21,22] In section 2, a first principle model developed with the commercial dynamic simulator Aspen Dynamics (Aspen Technology) is used to evaluate the predictive capabilities of the nonlinear wave model. Although the wave model captures the essential column dynamics, the composition profiles produced by the Aspen simulator exhibit self-sharpening behavior be-

* To whom correspondence should be addressed. Tel.: (413) 545-3481. Fax: (413) 545-1647. E-mail: henson@ecs.umass.edu.

10.1021/ie034320d CCC: $30.25
Published on Web 12/04/2004

cause of the nonlinear equilibrium relationship as well as wave distortion near the ends of the column. These effects are not captured by the wave model because of the assumption that the wave front has a constant shape.

These simulation results motivate the development of online parameter estimation strategies that allow the wave model to more closely match available measurements. The wave profile equation contains three parameters that characterize the wave slope and the asymptotic limits of the profile. Online estimation of these wave parameters has been previously investigated for other types of binary distillation columns. Rehm and Allgower[39] directly calculate the profile limit parameters from online measurements of the overhead and bottom compositions. Balasubramhanya and Doyle[1] propose the use of a linear Kalman filter for online estimation of the unmeasured wave profile position and the wave slope parameter from overhead and bottom composition measurements.

We present an alternative estimation strategy for nonlinear wave models in section 3. Rather than a simple adjustment of the wave model parameters to match overhead and bottom composition measurements, the use of online estimation to match the entire composition profile and improve prediction accuracy is explored. Because a typical nitrogen purification column only has a single composition measurement of the overhead vapor, we develop a systematic methodology for placement of additional measurements along the column that allow reconstruction of dynamic composition profiles. State and parameter estimation are performed using an extended Kalman filter (EKF)[8,15,28] that accounts for severe column nonlinearities present at very high nitrogen product purities. Other advantages of the EKF approach include the following: (1) restrictive assumptions on the model structure required in other nonlinear state estimation techniques[4,17,26,43] are not necessary; (2) measurements with different sampling frequencies and analysis delays can be handled;[6,30,32,36,42] (3) online computational demands are much less than those for nonlinear receding horizon estimators.[25,37,38]

The primary motivation for nonlinear wave modeling is the derivation of low-order distillation column models for nonlinear control system design. Wave models are used by Luyben[19] and Gilles and Retzbach[9] to develop control strategies for distillation columns with sharp temperature profiles. Balasubramhanya and Doyle utilize wave models within the input−output linearization framework to design nonlinear controllers for high-purity continuous[1] and batch reactive[2] distillation columns. Park and co-workers[10,14] present a closely related scheme in which the nonlinear wave model is used to design a generic model controller for profile position control. Rehm and Allgower[39] incorporate a wave model within the nonlinear H_∞ framework to achieve dual composition control.

In section 4, we present an alternative control strategy in which our nitrogen column wave model[44] is used to design a nonlinear model predictive controller for regulation of the overhead product purity. As compared to the controller design methods discussed above, nonlinear model predictive control (NMPC) is advantageous because process constraints and economic objectives can be included directly in the online optimization problem.[7,35] Nagy and co-workers[31] have presented a sophisticated computational method for a real-time solution of the relatively large NMPC problems that result when fundamental distillation column models are utilized for controller design. While the initial results are quite promising, the complexity of column configurations utilized in air separation plants appears to preclude successful application of this approach. We admit that the high complexity of a nonlinear model predictive controller is probably not justified for a simple nitrogen production plant. On the other hand, the potential economic benefits for triple column plants with higher value argon products are substantial. Therefore, the work described in the remainder of this paper should be viewed as a first step toward solving the triple column plant control problem.

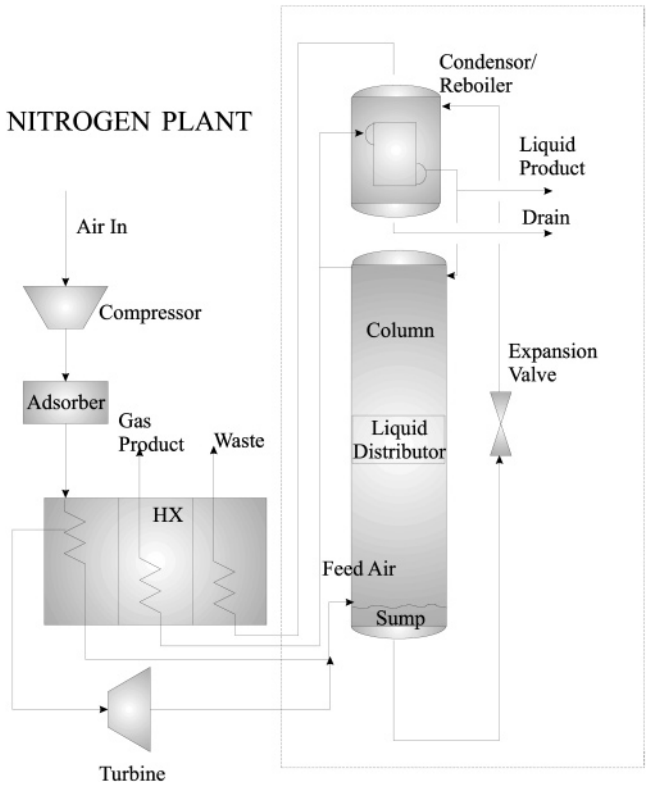

Figure 1. Schematic diagram of the nitrogen production plant.

2. Nitrogen Column Modeling

The major equipment for a typical nitrogen production plant are shown in Figure 1. The feed air stream is compressed to a pressure of 4−8 bar, and impurities such as water and carbon dioxide are removed via adsorption. The purified feed stream is cooled by column waste and product streams in a multipass heat exchanger. A portion of the feed stream is expanded across a turbine to provide additional cooling. The combined feed stream is introduced to the bottom of a packed column with 42 theoretical stages numbered sequentially from the top of the column. A sump located below the feed stage contains accumulated liquid from the bottom of the column. A liquid distributor located in the middle of the column is used to improve the flow characteristics of the descending liquid. The bottom liquid stream is expanded across a valve and partially liquified to produce a two-phase stream with a lower temperature than the overhead stream. In the combined condenser/reboiler, the partially liquified bottom stream is vaporized and the nitrogen vapor stream from the top

Table 1. Nominal Operating Conditions

variable	symbol (units)	value
feed flow rate	F (kmol/h)	98.4
feed vapor fraction	q (kmol/kmol)	0.963
feed O_2 composition	z_f (kmol/kmol)	0.2096
top-stage vapor composition	y_{out} (ppm)	2.81
average liquid holdup on each stage	n_l (kmol)	0.0852
average vapor holdup on each stage	n_v (kmol)	0.0186
liquid product flow rate	LN2 (kmol/h)	0.117
vapor product flow rate	GN2 (kmol/h)	49.134
reflux flow rate	L (kmol/h)	45.508

of the column is condensed to produce the reflux stream and liquid-nitrogen product stream. A portion of the column overhead stream is withdrawn as the gaseous nitrogen product.

The equipment inside the dashed lines of Figure 1 including the cryogenic column, the combined condenser/reboiler, and the expansion valve were modeled in our previous work.[44] In this study, the plant model is further simplified by neglecting the dynamics of the combined condenser/reboiler system. The primary motivation for this simplification is that the condenser/reboiler model is considerably more complex than the wave model of the nitrogen column. Through neglect of the condenser/reboiler dynamics, the nonlinear estimator and controller design problems are simplified considerably. Even though the condenser holdup is approximately 50% of the total process holdup, we have found that modeling errors introduced through neglect of condenser dynamics can be adequately compensated for through the use of nonlinear state and parameter estimation. Assuming that the temperature of the partially liquified bottom stream is sufficiently low that the overhead vapor stream is completely condensed, expansion valve and reboiler modeling are not necessary because only gaseous and liquid waste streams exit the reboiler. Results from the Aspen simulator discussed below show that this assumption is satisfied for any reasonable operating condition. As a result of these modeling simplifications, the transient compositions of the overhead vapor stream and the liquid product/reflux streams are identical in the simplified wave model used for nonlinear estimator and controller design.

2.1. Aspen Dynamic Simulator. Aspen Dynamics (Aspen Technology) was used to develop a rigorous dynamic simulation of the equipment located inside the dashed lines of Figure 1. The Aspen column model RadFrac solves the dynamic component balances and steady-state energy balances for each separation stage. The thermodynamic models used are nonrandom two liquid for the liquid phase and Peng−Robinson for the vapor phase. Proprietary thermodynamic property data for the air components (nitrogen, oxygen, and argon) were provided by Praxair, Inc. Equipment specifications and the steady-state operating conditions listed in Table 1 were obtained from a typical Praxair nitrogen plant. The Aspen simulator was used to represent the nitrogen plant in our estimation and control studies. To evaluate the modeling and control strategies over a reasonable range of operating conditions, four other steady states corresponding to feed flow rate changes of ±5 and ±10 kmol/h from the nominal value also were investigated.

2.2. Nonlinear Wave Model. The nonlinear wave model is based on several common assumptions including constant molar overflow, constant molar holdup, constant relative volatility, and perfect stage efficiency. The interested reader is referred to our original paper[44] for validation of these assumptions. Because the oxygen impurity in the nitrogen product stream is typically measured and controlled, a pseudobinary mixture is constructed by combining nitrogen and argon into a single component that is simply called "nitrogen" in the sequel.

The oxygen vapor composition y is described by the wave profile equation

$$y(z) = y_{min} + \frac{y_{max} - y_{min}}{1 + \exp[\gamma(z - s)]} \tag{1}$$

where $z \in [0, 1]$ is the scaled distance along the column with $z = 0$ representing the bottom, s is the wave position, γ is a slope parameter, and y_{min} and y_{max} are lower and upper asymptotic limits, respectively. Through neglect of the condenser/reboiler system and the expansion value, our previously developed wave model[44] can be reduced to a single ordinary differential equation and six algebraic equations expressed in terms of oxygen compositions:

$$w = \frac{ds}{dt} = \frac{1}{N_t} \frac{-L(x_{in} - x_{out}) + qF(y_{out} - y_{in})}{n_l(x_{in} - x_{out}) + n_v(y_{out} - y_{in})} \tag{2}$$

$$y_{out} = y_{min} + \frac{y_{max} - y_{min}}{1 + \exp[-\gamma(1 - s)]} \tag{3}$$

$$y(0) = y_{min} + \frac{y_{max} - y_{min}}{1 + \exp(\gamma s)} \tag{4}$$

$$x_{out} = \frac{y(0)}{\alpha - (\alpha - 1)y(0)} \tag{5}$$

$$y_{in} = \frac{\alpha x_f}{1 + (\alpha - 1)x_f} \tag{6}$$

$$Fz_f + Lx_{out} = qFy_{in} + [(1 - q)F + L]x_f \tag{7}$$

$$x_{in} = y_{out} \tag{8}$$

where w is the wave velocity, F, q, and z_f are the flow rate, vapor fraction, and composition of the feed air stream, respectively, L and qF are the internal liquid and vapor flow rates, respectively, N_t is the total number of equilibrium stages, n_l and n_v are the liquid and vapor holdups, respectively, associated with a single stage, x_{in} and x_{out} are the liquid compositions entering and exiting the column, respectively, y_{in} and y_{out} are the vapor compositions entering and exiting the column, respectively, $y(0)$ is the vapor composition in equilibrium with the liquid composition x_{out}, x_f is the feed-stage liquid composition in equilibrium with y_{in}, and α is the relative volatility. The model is comprised of the wave velocity equation (eq 2), the wave profile equation expressed at the top (eq 3) and bottom (eq 4) of the column, the equilibrium relation expressed at the bottom of the column (eq 5) and the feed stage (eq 6), a steady-state mass balance for the feed stage (eq 7), and the trivial equation (eq 8) for the combined condenser/reboiler. The fast dynamics of the feed stage relative to the overall column dynamics justifies the steady-state feed-stage balance. As discussed in our original paper,[44] the algebraic equations (3)−(7) can be manipulated such that the model is reduced to a single differential equation for the wave position s.

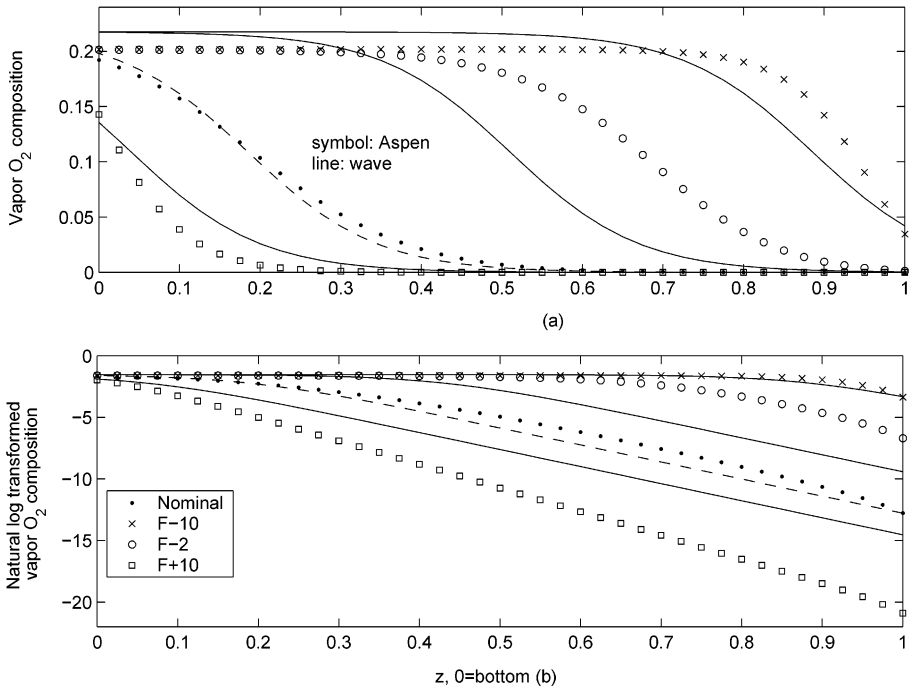

Figure 2. Open-loop simulation without wave model adaptation.

Figure 2 provides a comparison of steady-state oxygen composition predictions from the nonlinear wave model and the Aspen simulator. The nominal operating conditions shown in Table 1 correspond to approximately 90% of the maximum column capacity, while the other cases correspond to feed flow changes of −2, −10, and +10 kmol/h from the nominal value. Results are presented for the actual oxygen composition (top plot) to show the basic profile shape and for the natural log transformed oxygen composition (bottom plot) to more clearly show predictions near the top of the column where the nitrogen product is withdrawn. The wave model parameters (γ, y_{min}, and y_{max}) were estimated offline using the Aspen composition profile obtained at the nominal operating conditions.[44] Large deviations between the Aspen and wave model profiles are observed for the other three steady states. The poor wave model predictions are attributable to the use of constant wave profile parameters. While the y_{min} value of zero is appropriate for all four profiles, different values of the slope γ and the upper asymptotic limit y_{max} are needed for each steady state.[44] Because the assumption of a constant profile shape is not easily relaxed within the wave modeling framework, an alternative approach for achieving satisfactory steady-state and dynamic agreement is needed.

3. Nonlinear State and Parameter Estimation

We propose online state and parameter estimation as a relatively simple approach for improving the predictive capability of the nonlinear wave model. The wave position (s) is an unmeasured state variable that must be estimated for implementation of the nonlinear model predictive controller. The profile parameters are considered as candidate estimated variables because they directly affect the wave shape. Because a zero value of the lower asymptotic limit (y_{min}) is satisfactory for a wide range of operating conditions (see Figure 2), only the wave slope (γ) and the upper asymptotic limit (y_{max}) are considered as potential estimated parameters. Different estimation problems are formulated according to the wave parameters estimated and the column measurements used to provide feedback. The combined state/parameter estimation problems are solved by treating the estimated parameters as unmeasured state variables within the extended Kalman filtering framework.[8,15,28]

The information required to generate state and parameter estimates such that the wave model dynamically tracks the Aspen composition profile is obtained by placing oxygen composition and/or temperature measurements along the column. Below we present a simple algorithm for ranking candidate measurement locations according to their usefulness for online estimation. The following combinations of estimated variables are investigated:

1. The wave position s, the wave slope γ, and the upper asymptotic limit y_{max}.

2. The wave position s and the wave slope γ. The motivation for eliminating the upper asymptotic limit y_{max} from consideration will be explained in the following section.

Figure 2 shows that measurements located in highly pinched regions where the composition profile is nearly flat do not provide useful information about the profile shape. Because the composition profile can move substantially in response to changes in column operating conditions, additional measurements that otherwise would be unnecessary may be required to generate reasonable estimates. An advantage of the proposed algorithm is that the number of ranked measurements can exceed the number of estimated variables. While singular value decomposition (SVD) also can be used to rank candidate measurements for estimator design,[20,33] these techniques have the disadvantage that the number of ranked measurements cannot exceed the number of estimated variables.

3.1. Measurement Placement. The liquid composition on each theoretical stage is considered as a potential measurement. Compositions are natural log trans-

Table 2. Measurement Selection for Three Estimated Variables (s, γ, and y_{max})

measurement sequence	1st	2nd	3rd	4th	5th	6th
SS0 (nominal)	1	32	40	25	36	15
SS1 ($F - 5$)	3	9	1	6	11	41
SS2 ($F - 10$)	1	7	4	2	5	8
SS3 ($F + 5$)	33	1	40	37	21	39
SS4 ($F + 10$)	30	38	40	1	21	35
averaged gain	1	33	12	40	3	41
SVD for SS0	1	32	40	N/A	N/A	N/A

formed because the oxygen content in the upper part of the column is at parts per million (ppm) levels. The objective is to rank the 42 candidate measurement locations according to their usefulness for online estimation of the wave position and the chosen profile parameters. The inference of unmeasured stage compositions from pressure-corrected temperature measurements is addressed in the next section.

A detailed description of the measurement placement algorithm is presented in appendix A. The algorithm is an extension of a parameter selection procedure recently developed in our group.[18] Measurement selection is based on the steady-state sensitivity matrix between the estimated variables and the candidate measurements. A measure of the overall gain between all of the estimated variables and each measurement is derived by applying principal component analysis (PCA)[5] to the sensitivity matrix. A second measure related to the degree of linear independence of the candidate measurements is computed by solving a set of minimum distance problems involving the sensitivity vectors. A ranking of the candidate measurements, which provides a reasonable tradeoff between the two measures, is generated iteratively. Because of the nonlinear nature of the wave model, the sensitivity matrix is (potentially strongly) dependent on the steady state used for gain computation. Consequently, measurement rankings are generated for several steady states to examine this effect.

Table 2 shows the results obtained with the proposed measurement ranking procedure when the wave position (s) and two wave parameters (γ and y_{max}) are considered as estimated variables. Shown are the first six measurement locations chosen for five steady states corresponding to the nominal operating conditions in Table 1 and ± 5 and ± 10 kmol/h changes in the nominal feed flow rate. The stages are numbered sequentially from the top of the column. Also presented in Table 2 are measurement rankings obtained when the proposed method is applied to an averaged sensitivity matrix produced by element-by-element averaging of the sensitivity matrices for the five steady states. Rankings obtained by applying a representative SVD-based method[20] to the sensitivity matrix for the nominal steady state are included to provide a basis for comparison.

The proposed method tends to select measurements that are located within unpinched regions of the column. For example, highly ranked measurements for the steady state corresponding to a -10 kmol/h change in the nominal feed flow rate are clustered near the top of the column where the wave front position is located. A notable exception to this trend is the consistent high ranking of the stage 1 composition measurement. This result is attributable to the large sensitivities obtained for the first stage when the composition measurements are natural log transformed. At the nominal steady state, the proposed technique yields the same ranking of the first three measurements as the SVD method. Although not shown here, similar results are obtained for the other four steady states. The advantage of the proposed method is that the number of ranked measurements can exceed the number of estimated variables. The motivation for constructing the averaged sensitivity matrix is to generate measurement locations that are useful for estimating the wave position and profile parameters over a wide range of operating conditions.

Table 3. Measurement Selection for Two Estimated Variables (s and γ)

measurement sequence	1st	2nd	3rd	4th	5th	6th
SS0 (nominal)	28	1	35	19	39	32
SS1 ($F - 5$)	3	7	1	2	5	10
SS2 ($F - 10$)	1	4	2	6	3	8
SS3 ($F + 5$)	27	38	1	35	40	18
SS4 ($F + 10$)	1	39	33	37	24	40
averaged gain	1	28	8	41	15	4
SVD for SS0	28	1	N/A	N/A	N/A	N/A

Table 3 shows measurement rankings when the wave position (s) and the wave slope parameter (γ) are treated as the only estimated variables. The results are qualitatively similar to those obtained with three estimated parameters. Elimination of the y_{max} parameter leads to a slight deemphasis of measurements located near the bottom of the column. At the nominal steady state, the proposed and SVD methods yield identical rankings of the first two measurements.

3.2. EKF Design. The EKF approach[8,15,28] is used to generate state and parameter estimates from online measurements. A typical nitrogen purification column is equipped with an online measurement of the oxygen impurity in the overhead product stream (y_{out}). This measurement is highly ranked for all five steady states listed in Tables 2 and 3. While the composition analyzer provides a continuous measurement, the system required to transport samples from the column to the analyzer may introduce a significant delay not considered in the measurement placement procedure. Nevertheless, the overhead vapor analyzer provides the only direct measurement of the product composition and is utilized for online estimation. The rankings in Tables 2 and 3 are used to select the additional measurement locations.

Plant economics dictate that the selected stage compositions be inferred from pressure-corrected temperature measurements. The composition inference method described in appendix B is based on a pseudobinary mixture in which argon is lumped together with nitrogen. We have found that this simplification introduces noticeable errors only in the upper part of the column where the oxygen composition is very low. Different EKF designs are presented below for the following cases:

1. All composition and/or temperature measurements are available instantaneously. This assumption is reasonable if the sampling delay associated with composition analysis is very small compared to the column response time. Otherwise, this case serves as a preliminary step toward solving the estimation problem with measurement delay.

2. The overhead vapor composition measurement is delayed, and the other measurements are delay-free. This more realistic case is appropriate if stage compositions are inferred from pressure-corrected temperatures.

The undelayed measurement case is formulated as follows. The estimated wave model parameters p are

considered as additional unmeasured state variables:

$$ds/dt = F(s,u,p) \tag{9}$$

$$dp/dt = 0 \tag{10}$$

$$y = G(s,p) \tag{11}$$

where the first equation represents the wave velocity equation (2), the second equation allows for parameter variations, the third equation represents the wave profile expression (1) written for each measurement location, and the manipulated input u is the overhead vapor flow rate. When the state vector is defined as $x = [s, p^T]^T$, the augmented system can be rewritten as

$$dx/dt = f(x,u) \tag{12}$$

$$y = g(x) \tag{13}$$

A first-order EKF is designed by relinearizing the augmented system equations about the current state estimate $\hat{s}(k)$ and parameter estimate $\hat{p}(k)$ at each sampling instant. The interested reader is referred elsewhere[8,15,28] for detailed descriptions of the EKF formulation.

The delayed measurement case is a conceptually straightforward extension of the undelayed measurement case presented above. Consider the temporally discretized versions of eqs 9 and 11, where only a subset of the measurements are delayed:

$$s(k+1) = \bar{F}[s(k),u(k),p(k)] \tag{14}$$

$$y_u(k) = G_u[s(k),p(k)] \tag{15}$$

$$y_d(k+\theta) = G_d[s(k),p(k)] \tag{16}$$

where y_u denotes a vector of undelayed measurements that represent stage compositions or temperatures, y_d denotes the delayed overhead composition measurement, and θ is the measurement delay expressed as an integer multiple of the estimator sampling time. The following augmented nonlinear model is constructed:

$$s(k+1) = \bar{F}[s(k),u(k),p(k)] \tag{17}$$

$$s_1(k+1) = s(k) \tag{18}$$

$$s_2(k+1) = s_1(k) \tag{19}$$

$$s_\theta(k+1) = s_{\theta-1}(k) \tag{20}$$

$$p(k+1) = p(k) \tag{21}$$

$$p_1(k+1) = p(k) \tag{22}$$

$$p_2(k+1) = p_1(k) \tag{23}$$

$$p_\theta(k+1) = p_{\theta-1}(k) \tag{24}$$

$$y_u(k) = G_u[s(k),p(k)] \tag{25}$$

$$y_d(k) = G_d[s_\theta(k),p_\theta(k)] \tag{26}$$

The augmented state vector is defined as

$$x(k) = [s(k), s_1(k), s_2(k), ..., s_\theta(k), p^T(k), p_1{}^T(k), p_2{}^T(k), ..., p_\theta{}^T(k)]^T \tag{27}$$

The undelayed nonlinear model that results from augmentation has the form

$$x(k+1) = \bar{f}[x(k),u(k)] \tag{28}$$

$$y(k) = g[x(k)] \tag{29}$$

where the output vector is defined as $y(k) = [y_u{}^T(k), y_d(k)]^T$.

The augmentation approach allows a first-order EKF to be designed as in the undelayed measurement case. However, the number of estimated variables is much larger in the delayed case if the time delay is large relative to the sampling time. This dimensionality increase leads to a more complex EKF, which requires an additional tuning effort. A basic requirement of the EKF approach is that the augmented dynamic nonlinear model is detectable. The augmented models presented above can be shown to be linearly detectable, which suggests nonlinear detectability over some domain.[28] The stable EKF performance achieved in the simulation studies presented in section 5 suggests that this domain is rather large.

4. NMPC

4.1. Controller Formulation. We utilize the nonlinear wave model to design a nonlinear model predictive controller[11,23] that regulates the oxygen impurity in the overhead vapor product stream by manipulation of the overhead vapor flow rate. The air feed flow rate is treated as a measured disturbance that determines the overall nitrogen production rate. We utilize a standard NMPC formulation[23] with the following enhancements:

1. Rather than assume the availability of an accurate model and full-state feedback, nonlinear state and parameter estimation are used to adjust the wave model to match temperature and/or composition measurements located along the column.

2. Rather than utilize a standard output disturbance model,[11,23] steady-state offset that results from plant/model mismatch is removed using a state disturbance model in which the EKF estimate of the wave position serves the role of the plant measurement.

The NMPC objective function is chosen as

$$\Phi(k) = \sum_{j=1}^{N} [y(k+j|k) - y_s(k)]^T \mathbf{Q} [y(k+j|k) - y_s(k)] + \sum_{j=1}^{N} \Delta u^T(k+j|k)\, \mathbf{S} \Delta_u(k+j|k) \tag{30}$$

where u is the overhead vapor flow rate, y is the overhead oxygen impurity, y_s is the overhead composition target, $\mathbf{Q}$ and $\mathbf{S}$ are the diagonal tuning matrices, and N is the prediction horizon over which the objective function is minimized. The symbol $y(k+j|k)$ denotes the predicted value of y at time $k + j$ based on information available at time k. A sequence of control moves are calculated by solving the following minimization problem at each time step k:

$$\min_{u(k|k),u(k+1|k),...,u(k+M-1|k)} \Phi(k) \tag{31}$$

where $M \leq N$ is the control horizon over which the inputs are optimized. Inputs beyond the control horizon remain constant: $\Delta u(k+j|k) = 0$, where $j \in [M, N]$.

Minimization is performed subject to a set of inequality and equality constraints. The overhead vapor flow rate is constrained to be within lower and upper limits: $u \in [0, 150]$ kmol/h. The lower bound represents a physical limit, while the upper bound is approximately 150% of the nominal value in Table 1. Constraints are placed on the wave position estimate ($\hat{s}$) to ensure that a reasonable wave profile is obtained in the event that stage measurements become located in highly pinched regions of the column. Because movement of the wave position outside the column is physically meaningful, conservative bounds are imposed to prevent numerical problems: $\hat{s} \in [-1, 2]$. The nonlinear model equations are discretized using orthogonal collocation on finite elements and posed as a set of equality constraints.[23] The resulting nonlinear programming problem is solved in Matlab using the routine fmincon.

4.2. State Disturbance Model. As formulated, the nonlinear model predictive controller will exhibit steady-state offset in the presence of plant/model mismatch due to a lack of integral action. The standard approach for incorporating integral action into a model predictive controller is through the design of a disturbance model that adjusts the output target $y_s(k)$.[29] For stable systems such as the nitrogen purification column, a simple output disturbance model is often sufficient:

$$y_s(k) = y_{ref}(k) - d(k) \tag{32}$$

$$d(k) = y_p(k) - y(k|k) \tag{33}$$

where $y_{ref}(k)$ is the overhead composition setpoint, $y_p(k)$ is the measured overhead composition, $y(k|k)$ is the predicted overhead composition from the nonlinear wave model, and $d(k)$ is an additive output disturbance. The output term in the objective function (30) becomes

$$y(k+j|k) - y_s(k) = y(k+j|k) - y_{ref}(k) + y_p(k) - y(k|k) \tag{34}$$

The output disturbance model eliminates offset only if the predicted outputs asymptotically approach the same constant value: $\lim_{k\to\infty}[y(k+j|k) - y(k|k)] = 0$, where $j \in [1, N]$. Under this condition, the output term converges to the setpoint tracking error, $y(k+j|k) - y_s(k) = y_p(k) - y_{ref}(k)$, and minimization of the objective function (30) yields offset-free setpoint tracking if the required steady-state input is within its constraints.

The aforementioned requirement on the predicted outputs is not generally satisfied when open-loop predictions are initialized with the EKF state and parameter estimates. The prediction equations can be written as

$$s(k+j|k) = \bar{F}[s(k+j-1|k), u(k+j-1|k), \hat{p}(k)], \quad s(k|k) = \hat{s}(k) \tag{35}$$

$$y(k+j|k) = G[s(k+j|k), \hat{p}(k)] \tag{36}$$

where $\hat{s}(k)$ and $\hat{p}(k)$ are the current EKF state and parameter estimates, respectively. When the EKF utilizes more measurements than the number of estimated variables, biased estimates are produced at some measurement location(s) because of a lack of degrees of freedom. As a result, the EKF measurement correction term does not converge to zero and the estimates do not correspond to a steady-state solution of the nonlinear model. As a result, the predicted outputs do not asymptotically approach the same constant value and the nonlinear model predictive controller exhibits steady-state offset.

The design of disturbance models that guarantee an offset-free performance of linear model predictive controllers has received some recent attention.[27,34] An important conclusion is that offset elimination can be ensured by the addition of integrating disturbance variables as long as the number of disturbances is equal to the number of measured outputs and the resulting augmented system is detectable. Offset can be removed with less integrating variables if an additional rank condition is satisfied.[34] The addition of disturbance variables is quite reasonable for empirical linear models where the model parameters have no direct physical significance. However, the estimation of additive disturbances is less desirable in physically based nonlinear models where meaningful parameters are available. In this paper we pursue an alternative approach that exploits the availability of the nonlinear wave model and the effect of model parameters on the composition profile. Rather than simply estimating additive disturbances that eliminate measurement prediction errors, we have identified model parameters that can be adjusted such that the predicted composition profile tracks the entire profile produced by a detailed Aspen simulator. Therefore, we require a disturbance model that eliminates offset in the presence of estimated wave model parameters.

To this end, we propose a state disturbance model in which the EKF estimate of the wave position $\hat{s}(k)$ plays the role of the plant measurement:

$$s(k+j|k) = \tilde{s}(k+j|k) + d_s(k) \tag{37}$$

$$d_s(k) = \hat{s}(k) - \tilde{s}(k|k) \tag{38}$$

where $\tilde{s}(k|k)$ is the current open-loop prediction of the wave position obtained using the EKF parameter estimates but not the EKF state estimate, $\tilde{s}(k+j|k)$ is the open-loop prediction of the wave position at time $k + j$ based on information available at time k, $s(k+j|k)$ is the predicted value of the wave position used to compute the column compositions via the profile equation (1), and $d_s(k)$ is an additive state disturbance. The output target is set equal to the setpoint: $y_s(k) = y_{ref}(k)$. As shown in appendix C, this state disturbance model eliminates steady-state offset under the assumption that the EKF estimate of the overhead composition is unbiased. While this assumption is not easy to prove rigorously, the EKF is easily tuned to achieve an unbiased overhead composition estimate because this variable is measured directly. If the composition analyzer that provides this measurement becomes biased, no disturbance estimation scheme will be capable of providing an offset-free performance because this composition is also the controlled output. Consequently, the assumption is not unreasonable and does not unduly restrict practical application of the proposed method. A schematic diagram of the complete control strategy including the disturbance estimation scheme is shown in Figure 3.

5. Simulation Results

The nonlinear state/parameter estimator and nonlinear model predictive controller are evaluated via a series of open-loop and closed-loop simulation studies. The following measurement combinations are considered:

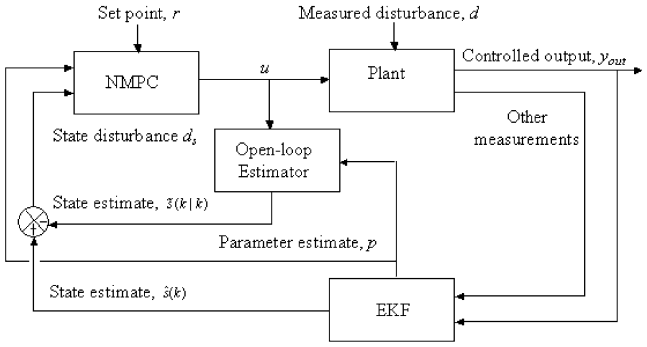

Figure 3. Schematic diagram of the proposed estimation and control scheme.

1. Delay-free composition measurements (Figures 4−7). This case provides an upper limit on an achievable estimator and controller performance.

2. Delay-free overhead composition and stage temperature measurements (Figure 8). This case is reasonable if the sampling system used for composition analysis has a negligible delay.

3. Delayed overhead composition and delay-free stage composition measurements (Figure 10). This case is a preliminary step toward the incorporation of delay-free stage temperature measurements.

4. Delayed overhead composition and delay-free stage temperature measurements (Figures 9 and 11). This case best represents an actual nitrogen purification column.

The measurement locations for each case are obtained from the averaged gain entries in Tables 2 and 3. All compositions are natural log transformed before being input to the nonlinear estimator and controller. Initial values of the estimated variables are obtained by fitting the wave profile expression (1) to Aspen composition data collected at the nominal steady state. The sampling time is chosen as $\Delta t = 0.01$ h, which is roughly 2.5% of the average open-loop time constant. This small sampling time was found to enhance estimator and controller stability. The EKF and nonlinear model predictive controller are implemented in Matlab, while the Aspen simulator is used to represent the column dynamics. The codes exchange information through Excel macros written in Microsoft Visual Basic.

We have found that the EKF must receive one more measurement than the number of estimated variables to produce reliable state and parameter estimates over a wide range of column operating conditions. Consequently, the EKF produces a biased estimate at one measurement location because of a lack of degrees of freedom. The EKF covariance matrices[28] were tuned by trial and error to produce an unbiased estimate of the overhead product composition to ensure an offset-free performance of the nonlinear model predictive controller. Additional tuning was performed to isolate bias to the measurement location furthest removed from the nominal wave position. EKF tuning is case-specific because of the different numbers and types of measurements employed in the various tests. While the EKF was easily tuned to yield an acceptable steady-state performance, considerable effort was required to determine tuning parameters that provided stable parameter estimates and rapidly converging predicted compositions. Approximately 20 dynamic simulation tests were performed for each measurement combination to determine a suitable set of tuning parameters. The resulting covariance matrices are not reported for the sake of brevity. By contrast, the nonlinear model predictive controller was readily tuned to provide an acceptable closed-loop performance over the wide range of operating conditions investigated.

5.1. Delay-Free Measurement Case. 5.1.1. Open-Loop Estimation. The EKF performance is evaluated for the idealized case where delay-free composition measurements are available for open-loop estimation.

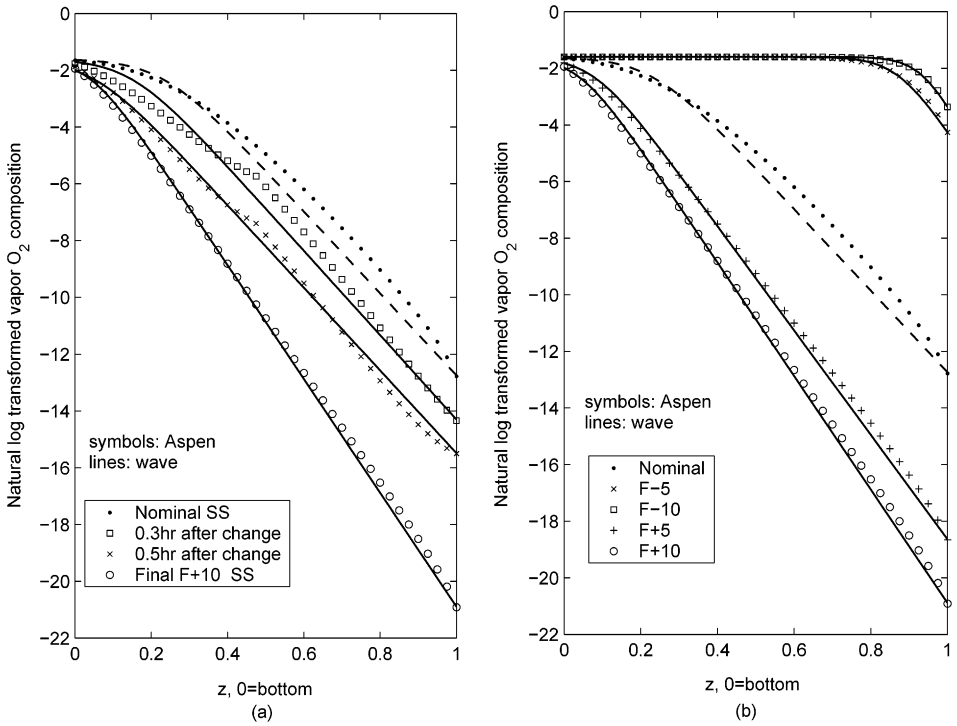

Figure 4. Open-loop estimation results for two estimated variables with three delay-free composition measurements: (a) dynamic vapor composition profiles for a $F + 10$ kmol/h step change in the feed flow rate; (b) estimated vapor composition profiles for five steady states.

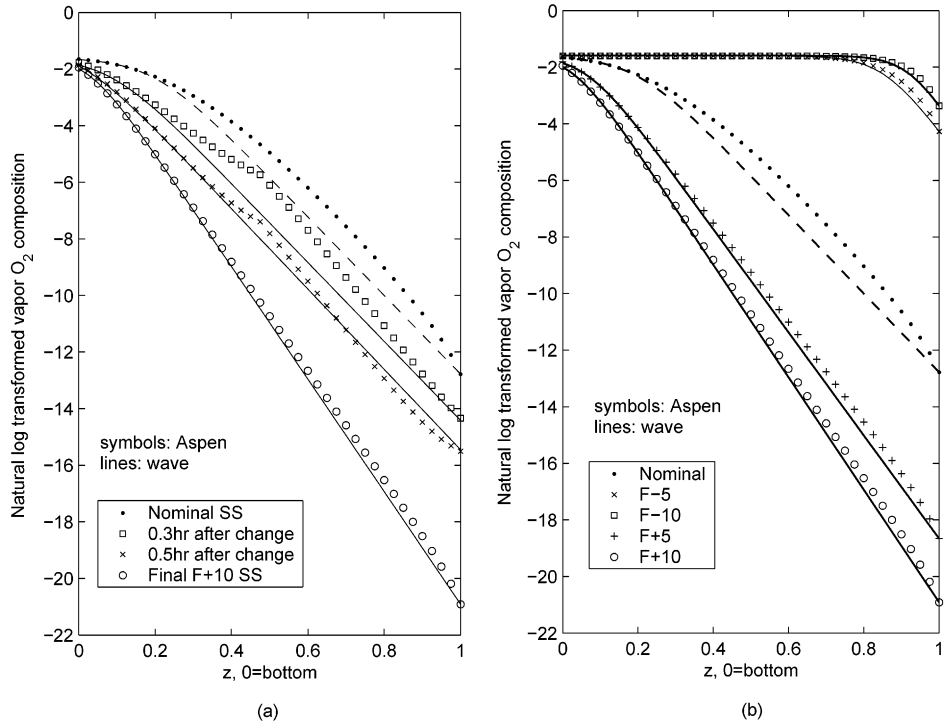

Figure 5. Open-loop estimation results for three estimated variables with four delay-free composition measurements: (a) dynamic vapor composition profiles for a $F + 10$ kmol/h step change in the feed flow rate; (b) estimated vapor composition profiles for five steady states.

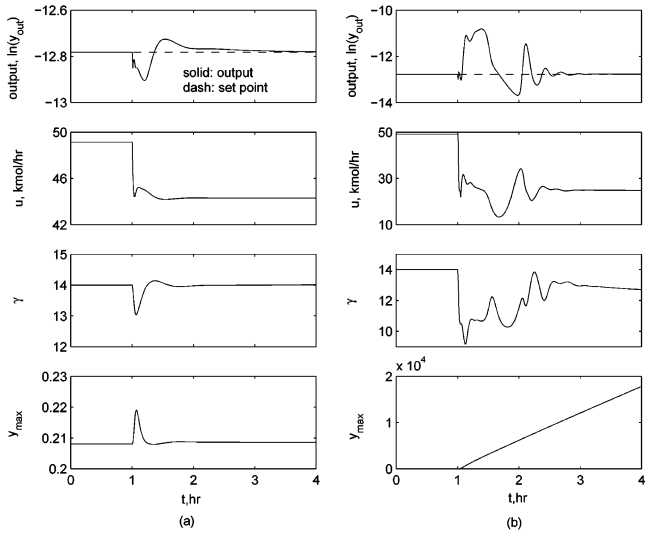

Figure 6. Closed-loop results for four delay-free composition measurements and three estimated variables: (a) −10% step disturbance in the feed flow rate; (b) −50% step disturbance in the feed flow rate.

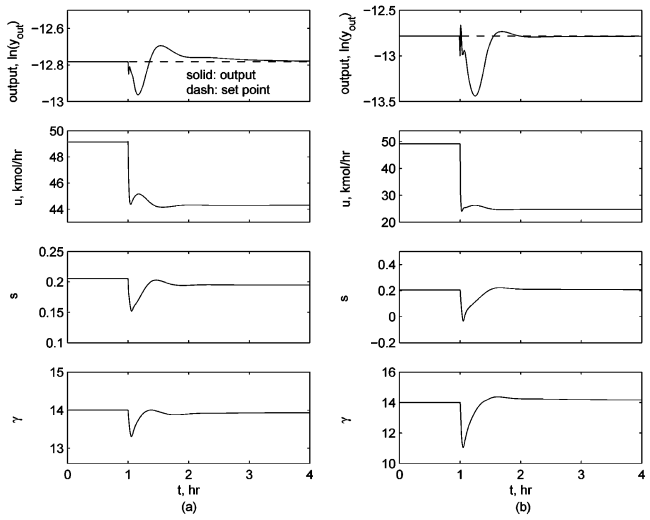

Figure 7. Closed-loop results for three delay-free composition measurements and two estimated variables: (a) −10% step disturbance in the feed flow rate; (b) −50% step disturbance in the feed flow rate.

Two scenarios are considered: (i) the wave position (s) and wave slope parameter (γ) are estimated from the overhead vapor composition measurement and liquid composition measurements located at stages 8 and 28 and (ii) the wave position, wave slope parameter, and upper asymptotic limit parameter (y_{max}) are estimated from the overhead vapor composition measurement and liquid composition measurements located at stages 12, 33, and 40. The first case represents the minimum number of estimated variables required for dynamic tracking of the composition profile. Addition of the estimated parameter y_{max} in the second case offers the potential for more accurate profile tracking. Stage composition measurements are taken from the liquid phase to simplify the associated sampling systems.

Figure 4a shows dynamic vapor composition profiles for two estimated variables when the feed air flow rate is increased by 10 kmol/h at time zero. Results are plotted in terms of the log transformed oxygen composition because the oxygen impurity is very small at the top of the column where the nitrogen product is withdrawn. The EKF provides good tracking of the composition profile at each time instant even though the upper part of the column is highly pinched at the final steady state. Figure 4b shows steady-state estimation results for five values of the feed flow rate (nominal and ±5 and ±10 kmol/h). The composition profile is accurately reconstructed at each steady state despite substantial changes in the wave position and significant variations in the wave shape. The corresponding results for three estimated parameters are shown in Figure 5. Addition

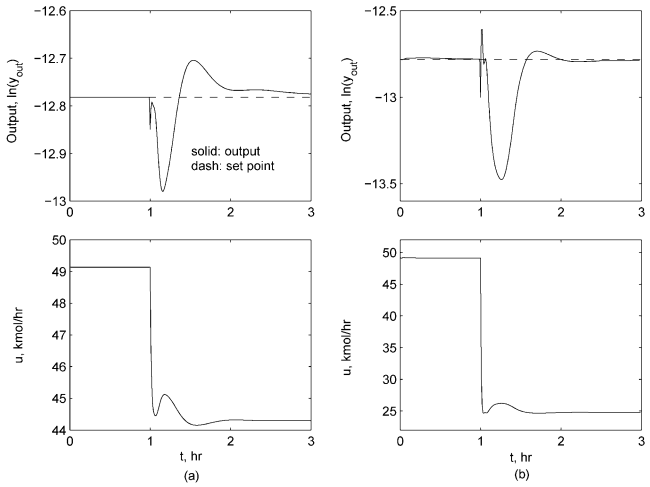

Figure 8. Closed-loop results for three delay-free composition and inferred composition measurements and two estimated variables: (a) −10% step disturbance in the feed flow rate; (b) −50% step disturbance in the feed flow rate.

of the second estimated parameter (y_{max}) yields only a slight improvement in dynamic predictions for the feed flow rate increase and very little improvement for reconstruction of the five steady-state profiles.

Although not shown here, the EKF performance is only slightly degraded when liquid composition measurements are replaced with pressure-corrected temperature measurements. The performance degradation is attributable to the assumption of a pseudobinary mixture in which argon is lumped together with nitrogen. Near the top of the column, the argon composition actually exceeds the oxygen composition by 3 orders of magnitude at the nominal steady state.

5.1.2. NMPC. The two EKFs with delay-free composition measurements are combined with a nonlinear model predictive controller that regulates the oxygen impurity in the overhead vapor stream by manipulation of the overhead vapor flow rate. The current estimate of the wave position $\hat{s}(k)$ is incorporated into the state disturbance model as shown in eqs 37 and 38, while the current parameter estimates $\hat{p}(k)$ are used directly to update the prediction model. The nonlinear model predictive controller is tuned as follows: $M = 2$, $N = 10$, $Q = 1$, and $R = 0.05$. A larger control horizon M yields little improvement in the closed-loop performance but significantly increases the computation time. Although the effective prediction horizon $N\Delta t = 0.1$ h is only about 25% of the average open-loop time constant, we found that larger N values offered negligible performance improvements.

Figure 6 shows closed-loop results when four delay-free composition measurements located at stages 1, 12, 33, and 40 are used to estimate the wave position (s) and two wave parameters (γ and y_{max}). Parts a and b of Figure 6 correspond to −10% and −50 measured disturbances, respectively, in the feed air flow rate at $t =$ 1 h. While these flow rate changes are somewhat modest compared to those encountered during plant startups and shutdowns, they serve to evaluate the performance of the nonlinear model predictive controller. The controlled output is plotted in log coordinates to more clearly show deviations from the setpoint. The combined estimator/controller is able to effectively reject the −10 disturbance shown in Figure 6a. While the two estimated parameters change to track the composition profile that temporarily moves downward in the column, they quickly stabilize at new values very close to their original steady-state values. This result indicates that

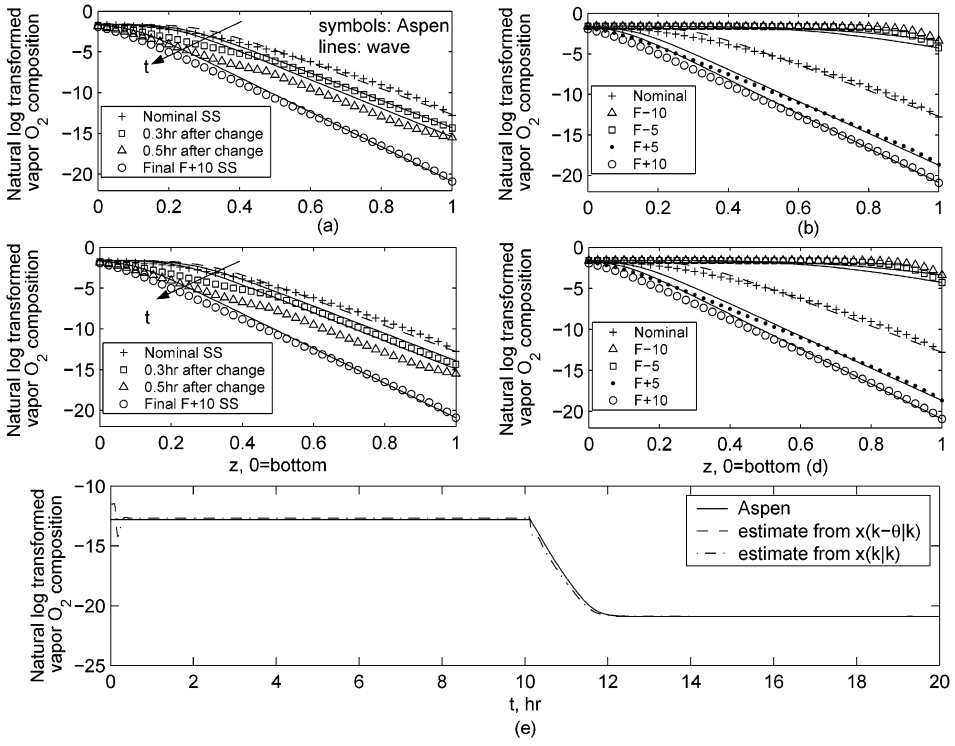

Figure 9. Open-loop estimation results for two estimated variables with one delayed composition measurement and two undelayed inferred composition measurements: (a) dynamic vapor composition profiles for a $F + 10$ kmol/h step change in the feed flow rate reproduced using $x(k|k)$; (b) steady-state vapor composition profiles reproduced using $x(k|k)$; (c) dynamic vapor composition profiles for a $F + 10$ kmol/h step change in the feed flow rate reproduced using $x(k-\theta|k)$; (d) steady-state vapor composition profiles reproduced using $x(k-\theta|k)$; (e) comparison of nitrogen product impurities predicted using $x(k-\theta|k)$ and $x(k|k)$.

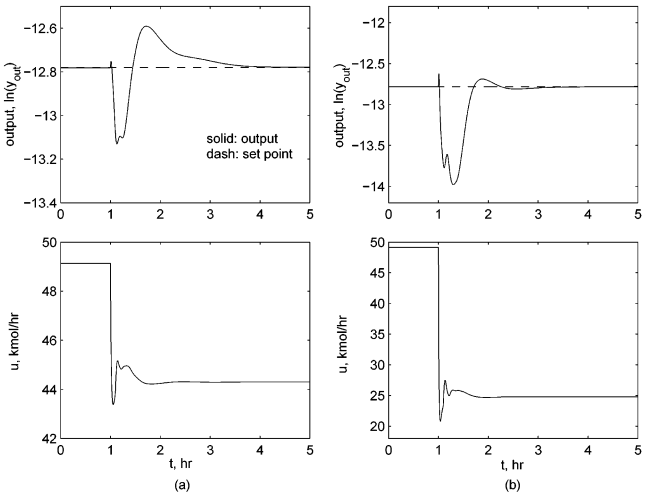

Figure 10. Closed-loop results for one delayed composition and two undelayed composition measurements and two estimated variables: (a) −10% step disturbance in the feed flow rate; (b) −50% step disturbance in the feed flow rate.

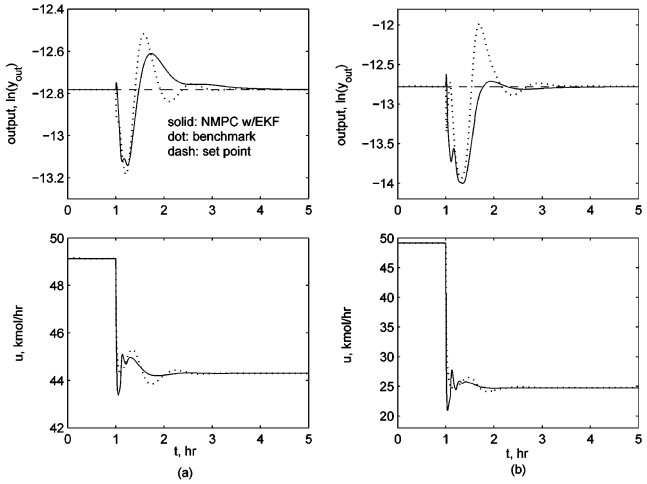

Figure 11. Closed-loop results for one delayed composition and two undelayed inferred composition measurements and two estimated variables: (a) −10% step disturbance in the feed flow rate; (b) −50% step disturbance in the feed flow rate.

composition profile movement is considerably less dramatic under NMPC than for open-loop operation. As a result, problems associated with measurements becoming located in highly pinched regions of the column are partially mitigated under closed-loop operation.

Figure 6b shows that larger feed flow rate disturbances can result in divergence of the EKF estimates and a poor NMPC performance. Divergence of the y_{max} estimate is attributable to the temporary movement of the composition profile downward in the column before control action can take effect. During this short time period, the wave position is located outside the physical column boundaries, and the two composition measurements at stages 1 and 12 no longer provide useful information for estimation. As a result, the y_{max} estimate starts to diverge and never returns to a physically meaningful value. Although not shown here, eventually the nonlinear model predictive controller fails because of the diverging parameter estimate. We have found that this problem cannot be solved by enforcing an upper limit on the parameter estimate or by adding additional measurements in the lower part of the column.

A simple solution to the divergence problem is to simply remove y_{max} as an estimated parameter. Figure 7 shows closed-loop results when three delay-free composition measurements located at stages 1, 8, and 28 are used to estimate the wave position (s) and the wave slope (γ). The results shown in Figure 7a for the −10% disturbance in the feed flow rate are qualitatively similar to those obtained with three estimated parameters. By contrast, Figure 7b shows that removal of y_{max} as an estimated parameter leads to a substantially improved controller performance for the −50% disturbance. Given that inclusion of a second estimated parameter increases the EKF complexity, necessitates a fourth-stage measurement, and yields a poor closed-loop performance for large feed flow rate changes, the remaining simulation tests will be performed with two estimated variables (s and γ).

Figure 8 shows the NMPC performance when the liquid composition measurements at stages 8 and 28 are replaced with pressure-corrected temperature measurements and the overhead vapor composition measurement remains undelayed. Despite the previously discussed problems with composition inference, the closed-loop performance is very similar to that in Figure 7 obtained with all composition measurements.

5.2. Delayed Measurement Case. 5.2.1. Open-Loop Estimation. The EKF performance is evaluated for the case where the overhead composition measurement is delayed by 0.09 h and pressure-corrected temperature measurements located on stages 8 and 28 are undelayed. Because a single wave parameter (γ) is estimated and the time delay $\theta = 9$, the augmented state is a 20-dimensional vector and the dimension of the EKF is increased commensurately. Figure 9 shows the results of open-loop estimation for a +10 kmol/h increase in the feed air flow rate when two different sets of state and parameter estimates are used for reconstruction of the composition profile. The results shown in Figure 9a,b are generated using $x(k|k)$, which represents the state and parameter estimates at time k based on measurements available at time k. Parts c and d of Figure 9 show the results obtained with $x(k-\theta|k)$, which represents the estimates at time $k - \theta$ based on measurements at time k. A comparison of parts a and c of Figure 9 shows that the wave profile generated with $x(k|k)$ provides superior dynamic tracking of the Aspen composition profile. However, composition profiles generated with $x(k|k)$ provide only marginally better agreement with Aspen data at the five previously investigated steady states, as shown in Figure 9b,d.

The motivation for including the results generated with the estimate $x(k-\theta|k)$ is shown in Figure 9e. This estimate produces almost perfect dynamic tracking and unbiased steady-state prediction of the Aspen product composition. By contrast, the estimate $x(k|k)$ yields noticeably faster dynamics and biased steady-state predictions. These results can be understood by recognizing that the current overhead composition measurement is the actual overhead composition θ time units in the past. Even though delay-free measurements of the stage temperatures are utilized, the information available at time k is only sufficient to produce unbiased estimates at time $k - \theta$. Because an unbiased estimate of the overhead vapor composition is necessary for the state disturbance model to eliminate steady-state offset, the closed-loop results presented in the next section are

Table 4. Comparison of Linear Benchmark and Nonlinear Controllers

controller	feed flow rate change	tracking error
benchmark	$F - 10\%$	20.807
NMPC	$F - 10\%$	21.223
NMPC with inference	$F - 10\%$	22.162
benchmark	$F - 50\%$	68.418
NMPC	$F - 10\%$	61.017
NMPC with inference	$F - 10\%$	56.511

generated by using the estimate $x(k-\theta|k)$ as an input to the nonlinear model predictive controller.

5.2.2. NMPC. The EKF with delayed overhead composition measurement is combined with the nonlinear model predictive controller described previously. Figure 10 shows closed-loop results when undelayed measurements of the stage 8 and 28 liquid compositions are assumed to be available. Parts a and b of Figure 10 correspond to −10% and −50% measured disturbances, respectively, in the feed air flow rate at $t = 1$ h. The nonlinear model predictive controller provides effective rejection of both disturbances even though the larger feed flow rate change causes dramatic movement of the composition profile under open-loop conditions. The degradation of the controller performance caused by the measurement delay is apparent when Figures 7 and 10 are compared. More specifically, the initial deviation from the setpoint is much larger and the settling time is slightly longer in the delayed measurement case.

Figure 11 shows the nonlinear model predictive controller performance when the liquid composition measurements at stages 8 and 28 are replaced with pressure-corrected temperature measurements. Results for −10% and −50% measured disturbances in the feed flow rate are shown in parts a and b of Figure 11, respectively. Also shown is the performance of a benchmark cascade controller that manipulates the overhead vapor flow rate using a delayed and log transformed feedback measurement of the overhead product composition and a feedforward measurement of the feed flow rate. The inner loop consists of a feedforward controller designed to maintain a constant ratio of the overhead vapor flow rate and the feed flow rate. The outer loop is a proportional−integral controller that maintains the overhead product composition at its setpoint by manipulating the setpoint of the ratio controller. Trial-and-error tuning of the cascade controller is used to achieve an acceptable compromise between the two peaks following the disturbance and the settling time.

Table 4 provides a quantitative comparison of the nonlinear model predictive and benchmark controllers using the sum of the absolute tracking errors as a measure of the closed-loop performance. Composition inference has a negligible effect on the NMPC performance for the smaller feed flow rate disturbance. The benchmark controller provides a slightly better performance for this case because column nonlinearities are not very pronounced. By contrast, the nonlinear model predictive controller with composition inference yields an improved performance as compared to the benchmark controller for the larger feed flow rate change. The lower error value obtained for the nonlinear model predictive controller is attributable to the smaller second peak following the disturbance. When the benchmark controller is retuned such that the second peak is comparable to that obtained with the nonlinear model predictive controller, the settling time becomes substantially longer and the error value is increased. Surprisingly, composition inference actually improves the performance of the nonlinear model predictive controller for this case.

6. Summary and Conclusions

A nonlinear wave model has been used to design nonlinear state/parameter estimators and a nonlinear model predictive controller for a simulated nitrogen purification column. Extended Kalman filtering was used to generate online estimates of the wave position and key wave profile parameters that allow the wave model to dynamically track composition profiles produced by a rigorous Aspen simulator. A new measurement selection technique was developed to determine the more favorable measurement locations for combined state and parameter estimation. The estimated variables serve as inputs to a nonlinear model predictive controller that regulates the oxygen impurity in the overhead nitrogen product by manipulating the overhead vapor flow rate. A state disturbance scheme was developed to allow the EKF estimates to be incorporated into the nonlinear model predictive controller without steady-state offset. Several EKF formulations that differ according to the number and type of available measurements were investigated.

The simulation results support the following conclusions:

1. One more measurement than the number of estimated variables is required for the EKF to robustly function over a wide range of column operating conditions. The measurement selection scheme provides a rational basis for determining the locations of these composition and/or temperature measurements.

2. Satisfactory open-loop predictions are obtained by estimating the wave position and the wave slope parameter. While the use of the upper asymptotic limit as an additional estimated parameter yields modest improvements in open-loop predictions, the estimate of this parameter can diverge when the EKF is combined with the nonlinear model predictive controller.

3. The EKF provides excellent tracking of Aspen composition profiles when delay-free composition measurements are available. Profile predictions are degraded when the overhead composition measurement is delayed and/or the intermediate-stage composition measurements are replaced by pressure-corrected temperature measurements.

4. The adapted wave model produces an accurate prediction of the overhead composition. As a result, an acceptable NMPC performance is obtained despite the aforementioned problems with composition profile prediction.

5. The nonlinear model predictive controller outperforms a benchmark cascade controller for large measured disturbances in the feed air flow rate. While the engineering effort required for controller development and maintenance is probably not economically justifiable for a simple nitrogen purification column, we believe that the use of nonlinear wave models within the EKF/NMPC framework holds promise for more complex triple column plants in the air separation industry.

Acknowledgment

Financial support from the National Science Foundation (Grant CTS-0241211) and Praxair, Inc., is grate-

fully acknowledged. The authors also thank Aspen Technology for providing the Aspen Engineering Suite software.

Appendix A: Measurement Selection Algorithm

1. Formulate the estimated variable/measured output gain matrix:

$$K_{ij} = \frac{\partial y_i / \bar{y}_i}{\partial p_j / \bar{p}_j} \tag{39}$$

where p_j, with $j \in [1, q]$, is the jth estimated variable (the wave position or a wave profile parameter), y_i, with $i \in [1, m]$, is the ith measured output (a stage composition), and $\bar{y}_i$ and $\bar{p}_j$ are nominal values corresponding to a particular steady-state operating point. A large sensitivity coefficient K_{ij} suggests that the output y_i provides useful information for the estimation of the variable p_j. The gain elements for the wave position (s) were calculated analytically, while the elements for the wave model parameters (γ and y_{max}) were determined using finite differences.

2. Perform PCA[5] on the covariance matrix: $\mathbf{X} = \mathbf{K}^T\mathbf{K} \in \mathbf{R}^{m \times m}$. Denote λ_i as the ith eigenvalue of $\mathbf{X}$ and c_{ji} as the jth element of the ith principle component. The weighted sum of the principle component elements and their corresponding eigenvalues

$$E_j = \frac{\sum_{i=1}^{m} |\lambda_i c_{ji}|}{\sum_{i=1}^{m} |\lambda_i|} \in [0, 1] \tag{40}$$

is a measure of the overall response of the jth measurement to variations in the estimated variables. Select the measurement with the largest E_j value as the first measurement location.

3. For the second to qth measurement locations, determine the smallest distance vector in the space spanned by the sensitivity vectors of the n measurements already chosen. Assume the sensitivity vectors s_k are linearly independent where $1 \le n < q$. Any vector $\bar{s}$ in the n-dimensional vector space $\mathbf{S}_n$ can be expressed as

$$\bar{s} = \sum_{k=1}^{n} a_k s_k \tag{41}$$

where the a_k's are constants. Consider the sensitivity vector s_j associated with a candidate measurement not already selected. The vector closest to s_j in the space $\mathbf{S}_n$ is determined as

$$\min_{a_k} \frac{1}{2}(s_j - \bar{s})^T(s_j - \bar{s}) \tag{42}$$

Compute the following measure $d_j \in [0, 1]$ that quantifies the degree of linear independence between the candidate sensitivity vector s_j and the minimum distance sensitivity vector $\bar{s}$:

$$d_j = \sin\left[\cos^{-1}\left(\frac{s_j^T - \bar{s}}{||s_j|| \cdot ||\bar{s}||}\right)\right] \tag{43}$$

where $||\cdot||$ represents the Euclidean norm. Measurements with large d_j values are favored for the selection because they provide unique information compared to the measurements already chosen. Calculate the identifiability indices $I_j = E_j d_j \in [0, 1]$. Select the measurement with the largest I_j value as the next measurement location.

For the $(q + 1)$th to mth measurement locations, form all possible $(p - 1)$-tuples of the previously selected measurements. The number of possible combinations is

$$r = \frac{k!}{(q-1)!(k-q+1)!}, \quad q + 1 \le k \le m \tag{44}$$

Use eq 43 to compute the linear independence metric $d_{r,j}$ with respect to the j candidate measurement location for all r possible combinations. Determine the worst case over all possible combinations: $d_j = I_j d_{r,j}$. Calculate the identifiability index I_j for each candidate measurement. Select the measurement with the largest I_j value as the next measurement location.

Appendix B: Composition Inference Procedure

The following assumptions are invoked: (1) the ternary mixture consisting of nitrogen, oxygen, and argon can be treated as a pseudobinary mixture in which argon is lumped together with nitrogen; (2) the ideal gas law holds for the pseudobinary mixture in the vapor phase; (3) the pseudobinary mixture forms an ideal solution in the liquid phase; (4) vapor−liquid equilibrium is established on each separation stage; and (5) the column pressure profile varies linearly between the known bottoms and overhead pressures. The following relationships can be derived from these assumptions:[41]

$$y_{i,1} P_i = x_{i,1} P^*_{i,1} \tag{45}$$

$$y_{i,2} P_i = x_{i,2} P^*_{i,2} \tag{46}$$

$$y_{i,1} + y_{i,2} = 1 \tag{47}$$

$$x_{i,1} + x_{i,2} = 1 \tag{48}$$

where i is the stage number, the subscripts 1 and 2 denote pure oxygen and nitrogen, respectively, x and y are the liquid and vapor compositions, respectively, P^* is the pure-component vapor pressure, and P is the total pressure. Pure-component vapor pressures are calculated using the Antoine equation:

$$P^*_{i,1} = \exp\left(A_1 - \frac{B_1}{T_i + C_1}\right) \tag{49}$$

$$P^*_{i,2} = \exp\left(A_2 - \frac{B_2}{T_i + C_2}\right) \tag{50}$$

where T is the absolute temperature. The Antoine constants A, B, and C shown in Table 5 were regressed from Aspen physical property data for pure oxygen and lumped nitrogen where the pressure and temperature

Table 5. Antoine Equation Constants

constant	pure O_2	lumped N_2
A	9.2109	10.4204
B	552.77	552.92
C	−2.7588	−4.6554

have units of psia and K, respectively. The total pressure is assumed to be known from a linear pressure profile, while stage temperatures obtained from the Aspen simulator at the nominal steady state are assumed to remain constant despite changes in the feed flow rate. The component vapor and liquid compositions can be calculated directly from the six equations listed above.

Appendix C: Analysis of the State Disturbance Model

The open-loop state prediction equations can be written as

$$\tilde{s}(k+j|k) = \bar{F}[\tilde{s}(k+j-1|k),u(k+j-1|k),\hat{p}(k)] \quad (51)$$

$$\tilde{s}(k|k) = \tilde{s}(k|k-1) = \bar{F}[\tilde{s}(k-1|k-1),u(k-1),\hat{p}(k-1)] \quad (52)$$

where $\tilde{s}(k-1|k-1)$ is the open-loop prediction obtained at the last iteration using the previous EKF parameter estimate $\hat{p}(k-1)$. Under the assumption that the closed-loop system is asymptotically stable, the EKF parameter estimate $\hat{p}(k)$ and the NMPC-calculated input moves $u(k+j-1|k)$ converge to constant values. Therefore, the open-loop state predictions also converge to a constant value: $\lim_{k\to\infty}[\tilde{s}(k+j|k) - \tilde{s}(k|k)] = 0$, with $j \in [1, N]$. In the limit as $k \to \infty$

$$s(k+j|k) = \tilde{s}(k+j|k) + \hat{s}(k) - \tilde{s}(k|k) = \hat{s}(k) \quad (53)$$

The open-loop prediction equation for the controlled output can be written as

$$y(k+j|k) = G[s(k+j|k),\hat{p}(k)] \Rightarrow \lim_{k\to\infty} y(k+j|k) = G[\hat{s}(k),\hat{p}(k)] \quad (54)$$

The first assumption, that the constant input that asymptotically minimizes the objective function (30) is unconstrained, implies $\lim_{k\to\infty}[y(k+j|k) - y_s(k)] = \lim_{k\to\infty}[y(k+j|k) - y_{ref}(k)] = 0$. The second assumption, that the controlled output prediction generated from the EKF estimates is unbiased, implies $\lim_{k\to\infty}\{y_p(k) - G[\hat{s}(k),\hat{p}(k)]\} = 0$. Consequently, the nonlinear model predictive controller eliminates steady-state offset: $\lim_{k\to\infty}[y_p(k) - y_{ref}(k)] = 0$.

Nomenclature

A, B, C = Antoine equation constants
F = feed air flow rate (kmol/h)
$\mathbf{K}$ = estimate output gain matrix
L = liquid molar flow rate (kmol/h)
M = control horizon
N = number of theoretical stages; prediction horizon
n_l = stage liquid holdup (kmol)
n_v = stage vapor holdup (kmol)
P = pressure (psia)
P^* = vapor pressure (psia)
p = vector of parameters
$\mathbf{Q}$ = output weighting matrix
q = feed air vapor fraction
$\mathbf{S}$ = input weighting matrix
s = wave front position
$\tilde{s}$ = open-loop estimate of the wave position
$\hat{s}$ = EKF estimate of the wave position
T = temperature (°C)
u = manipulated input
V = vapor molar flow rate (kmol/h)
w = wave propagation velocity (h^{-1})
x = liquid composition; state vector
x_f = feed-stage liquid composition
x_{in} = liquid composition entering the column section
x_{out} = liquid composition exiting the column section
$\hat{x}$ = state estimate
y = vapor composition
y_{in} = vapor composition entering the column section
y_{out} = vapor composition exiting the column section
y_{min} = lower asymptotic limit of the vapor composition profile
y_{max} = upper asymptotic limit of the vapor composition profile
$\hat{y}$ = output estimate
z = dimensionless spatial coordinate
z_f = feed air oxygen composition
α = relative volatility
γ = wave front slope
θ = time delay of the discretized model

Literature Cited

(1) Balasubramhanya, L. S.; Doyle, F. J. Nonlinear control of a high-purity distillation column using a traveling-wave model. *AIChE J.* **1997**, *43*, 703−714.

(2) Balasubramhanya, L. S.; Doyle, F. J. Nonlinear model-based control of a batch reactive distillation column. *J. Process Control* **2000**, *10*, 209−218.

(3) Barron, R. F. *Cryogenic Systems*; Oxford Press: New York, 1985.

(4) Bastin, G.; Gevers, M. R. Stable adaptive observers for nonlinear time-varying systems. *IEEE Trans. Autom. Control* **1988**, *AC-33*, 650−658.

(5) Dunteman, G. H. *Principal Components Analysis*; Sage Publications Inc.: Newbury Park, CA, 1989.

(6) Ellis, M. F.; Taylor, T. W.; Gonzales, V.; Jensen, K. F. Estimation of molecular weight distribution in batch polymerization. *AIChE J.* **1988**, *34*, 1341−1353.

(7) Ganguly, S.; Saraf, D. N. Startup of a distillation column using nonlinear analytical model predictive control. *Ind. Eng. Chem. Res.* **1993**, *32*, 1667−1675.

(8) Gelb, A. *Applied Optimal Estimation*; MIT Press: Cambridge, MA, 1974.

(9) Gilles, E. D.; Retzbach, B. Reduced models and control of distillation columns with sharp temperature profiles. *IEEE Trans. Autom. Control* **1983**, *28*, 628−630.

(10) Han, H.; Park, S. Profile position control of batch distillation based on a nonlinear wave model. *Ind. Eng. Chem. Res.* **2001**, *23*, 187−202.

(11) Henson, M. A. Nonlinear model predictive control: Current status and future directions. *Comput. Chem. Eng.* **1998**, *23*, 187−202.

(12) Hwang, Y. L. Nonlinear wave theory for dynamics of binary distillation column. *AIChE J.* **1991**, *37*, 705−723.

(13) Isalski, W. H. *Separation of Gases*; Oxford Press: New York, 1989.

(14) Han H.; Shin, J.; Seo, H.; Park, S. A nonlinear profile observer using tray temperatures for high-purity distillation column control. *Chem. Eng. Sci.* **2000**, *55*, 807−816.

(15) Jazwinski, A. H. *Stochastic Processes and Filtering Theory*; Academic Press: New York, 1970.

(16) Kienle, A. Lower-order dynamic models for ideal multicomponent distillation process using nonlinear wave propogation theory. *Chem. Eng. Sci.* **2000**, *55*, 1817−1828.

(17) Krener, A. J.; Isidori, A. Linearization by output injection and nonlinear observers. *Syst. Control Lett.* **1983**, *3*, 47−52.

(18) Li, R.; Henson, M. A.; Kurtz, M. J. Selection of model parameters for off-line parameter estimation. *IEEE Trans. Control Systems Technol.* **2004**, *12*, 402-412.

(19) Luyben, W. L. Profile position control of distillation columns with sharp temperature profiles. *AIChE J.* **1972**, *18*, 238.

(20) Luyben, W. L. *Process Modeling, Simulation and Control for Chemical Engineers*; McGraw-Hill: New York, 1973.

(21) Marquardt, W. Nonlinear model reduction for binary distillation. *Proceedings of IFAC Control of Distillation Columns and Chemical Reactors*; Bournemouth, U.K., 1986; pp 123−128.

(22) Marquardt, W.; Amrhein, M. Development of a linear distillation model from design datafor process control. *Comput. Chem. Eng.* **1994**, *18*, S349−S353.

(23) Meadows, E. S.; Rawlings, J. B. Model predictive control. In *Nonlinear Process Control*; Henson, M. A., Seborg, D. E., Eds.; Prentice-Hall: Englewood Cliffs, NJ, 1997; Chapter 5, pp 233−310.

(24) Meziou, A. Z. The application of multivariable constrained control to cryogenic air separation units. ISA Expo/2000, 2000.

(25) Michalska, H.; Mayne, D. Q. Moving horizon observers and observer-based control. *IEEE Trans. Autom. Control* **1995**, *40*, 995−1006.

(26) Moraal, P. E.; Grizzle, J. W. Observer design for nonlinear systems with discrete-time measurements. *IEEE Trans. Autom. Control* **1995**, *AC-40*, 395−404.

(27) Muske, K. R.; Badgwell, T. A. Disturbance modeling for offset-free linear model predictive control. *J. Process Control* **2002**, *12*, 617−632.

(28) Muske, K. R.; Edgar, T. F. Nonlinear state estimation. In *Nonlinear Process Control*; Henson, M. A., Seborg, D. E., Eds.; Prentice-Hall: Englewood Cliffs, NJ, 1997; Chapter 6, pp 311−370.

(29) Muske, K. R.; Rawlings, J. B. Model predictive control with linear models. *AIChE J.* **1993**, *39*, 262−287.

(30) Mutha, R. K.; Cluett, W. R.; Penlidis, A. On-line model-based estimation and control of a polymer reactor. *AIChE J.* **1997**, *43*, 3042−3058.

(31) Nagy, Z.; Findeisen, R.; Diehl, M.; Allgower, F.; Bock, H. G.; Agachi, S.; Schlooder, J. P.; Leineweber, D. Real-time feasibility of nonlinear predictive control for large scale processes—A case study. *Proceedings of the American Control Conference*, Chicago, IL, 2000; pp 4249−4254.

(32) Ogunnaike, B. A. On-line modelling and predictive control of an industrial terpolymerization reactor. *Int. J. Control* **1994**, *59*, 711−729.

(33) Oisiovici, R. M.; Cruz, S. L. Inferential control of high-purity multicomponent batch distillation columns using an extended Kalman filter. *Ind. Eng. Chem. Res.* **2001**, *40*, 2628−2639.

(34) Pannocchia, G.; Rawlings, J. B. Disturbance models for offset-free model-predictive control. *AIChE J.* **2003**, *49*, 426−437.

(35) Patwardhan, A. A.; Edgar, T. F. Nonlinear model predictive control of a packed distillation column. *Ind. Eng. Chem. Res.* **1993**, *32*, 2345−2356.

(36) Prasad, V.; Schley, M.; Russo, L. P.; Bequette, B. W. Product property and production rate control of styrene polymerization. *J. Process Control* **2002**, *12*, 353−372.

(37) Rao, C. V.; Rawlings, J. B. Nonlinear moving horizon estimation. In *Nonlinear Model Predictive Control*; Allgower, F., Zheng, A., Eds.; Birkhauser: Basel, Switzerland, 2000; pp 45−69.

(38) Rao, C. V.; Rawlings, J. B.; Mayne, D. Q. Constrained state estimation for nonlinear discrete-time systems: Stability and moving horizon approximations. *IEEE Trans. Autom. Control* **2003**, *48*, 246−258.

(39) Rehm, A.; Allgower, F. Nonlinear H_∞-control of a high purity distillation column. *UKACC International Conference on Control '96*; Exeter, U.K., 1996; pp 1178−1183.

(40) Roel, B.; Betlem, B. H. L.; de Ruijter, J. A. F. First principles dynamic modeling and multivariable control of a cryogenic distillation process. *Comput. Chem. Eng.* **2000**, *24*, 111−123.

(41) Smith, J. M.; Van Ness, H. C. *Introduction to Chemical Engineering Thermodynamics*; McGraw-Hill: New York, 1975.

(42) Tatiraju, S.; Soroush, M.; Ogunnaike, B. A. Multirate nonlinear state estimation with application to a polymerization reactor. *AIChE J.* **1999**, *45*, 769−780.

(43) Zeitz, M. The extended Luenberger observer for nonlinear systems. *Syst. Control Lett.* **1987**, *9*, 149−156.

(44) Zhu, G.-Y.; Henson, M. A.; Megan, L. Low-order dynamic modeling of cryogenic distillation columns based on nonlinear wave phenomenon. *Sep. Purif. Technol.* **2001**, *24*, 467−487.

Received for review December 17, 2003
Revised manuscript received August 22, 2004
Accepted October 25, 2004

IE034320D